Flash-Photolysis of Fully Reduced and Mixed-Valence CO-Bound *Rhodobacter sphaeroides* Cytochrome *c* Oxidase: Heme Spectral Shifts†

Istvan Szundi,‡ Jayashree Ray,‡ Ashtamurthy Pawate,§ Robert B. Gennis,§ and Ólöf Einarsdóttir*,‡

Department of Chemistry and Biochemistry, University of California, Santa Cruz, California 95064, and Department of Biochemistry, University of Illinois, Urbana Champaign, Illinois 61801

Received April 17, 2007; Revised Manuscript Received August 22, 2007

ABSTRACT: Conformational changes, internal electron transfer, and CO rebinding processes in cytochrome *c* oxidase from *Rhodobacter sphaeroides* reduced to different degrees were investigated. The reactions were followed using a gated optical spectrometric multichannel analyzer. Light-induced difference spectra, recorded in the 350−700 nm region over the 100 ns to 1 s time interval, were analyzed by singular value decomposition and global exponential fitting. The photolyzed fully reduced enzyme showed two relaxations, ∼1 and 190 μs, prior to the 20 ms CO rebinding process. Intramolecular electron transfer was monitored following photolysis of the mixed-valence CO-bound enzyme. The analysis revealed 1.1 μs, 2.4 μs, 31 μs, 68 ms, and 240 ms apparent lifetimes, the first three of which are attributed to electron transfer from heme a_3 to heme *a* with contribution from a relaxation process at the heme a_3 site. Spectral changes associated with the microsecond processes are consistent with 75% electron transfer from heme a_3 to heme *a*. A comparison of the experimental spectra and model difference spectra for the intramolecular electron transfer indicated ∼3 nm blue shift in the absolute spectra of both the oxidized heme a_3 and reduced heme *a* generated in the process. The 68 and 240 ms lifetimes are due to CO recombination to heme a_3 and are attributed to the presence of two conformers, the slower rate corresponding to the conformer in higher abundance. The dependency of the apparent rate of CO rebinding on the intensity of the probe beam in single-wavelength experiments is explained.

Intramolecular electron transfer in both bovine heart and *Rhodobacter sphaeroides* cytochrome *c* oxidase in the absence of dioxygen has previously been investigated by photolyzing the mixed-valence CO-bound enzymes and monitoring the back-flow of electrons from the reduced binuclear center to the oxidized heme *a* and Cu_A[1] (*1*−*11*). In the *R. sphaeroides* enzyme, three kinetic processes with apparent lifetimes of 3 μs, 35 μs, and 1 ms were reported and attributed to electron transfer from heme a_3 to heme *a*, subsequent electron transfer to Cu_A, and an additional pH-dependent electron transfer from heme a_3 to heme *a*, respectively (*11*). These events are similar to those reported for the bovine enzyme (*5*, *8*, *9*, *10*). However, in the *R. sphaeroides* enzyme, the extent of electron back-flow from heme a_3 to heme *a* on the 3−5 μs time scale was reported to be three times larger than for the bovine enzyme (*11*). Apparent rate constants of 50 and 15 s^{-1} were reported for the CO recombination in the mixed-valence bovine and *R. sphaeroides* enzymes, respectively, with the slower rate resulting from greater electron back-flow in the bacterial enzyme (*11*). These studies were carried out at a few selected wavelengths and provided important information regarding the rates of the proposed processes. However, the absorption spectra of the individual intermediates themselves, a direct proof of the mechanism, could not be identified due to limited spectral information, and thus specific questions regarding the intermediates could not be addressed.

Our laboratory has previously investigated intramolecular electron transfer in the bovine enzyme following photolysis of CO-bound mixed-valence and three-electron-reduced enzyme using an intensified diode array (*8*, *10*). Time-resolved optical absorption difference spectra over broad spectral and time ranges were obtained, and singular value decomposition (SVD), global exponential fitting, and further kinetic analysis allowed us to deduce spectra of the postulated intermediates involved in the electron back-flow (*8*, *10*).

In this study, we used multichannel detection to monitor spectral changes generated following photolysis of CO-bound cytochrome *c* oxidase from *R. sphaeroides* reduced to different degrees. In the mixed-valence enzyme, three processes involving electron transfer from heme a_3 to heme *a* on a microsecond time scale were observed. The data suggest 3−4 nm shifts in the spectra of the oxidized heme a_3 and reduced heme *a*, which are generated upon electron transfer. The shifts, which were determined by simulation using Gaussian curves, may be the result of a structural change near the hemes. The CO recombination in the mixed-

† This work was supported by National Institutes of Health (NIH) Grant GM 53788 (Ó.E.) and NIH Grant HL16101 (R.B.G.).

* Author to whom correspondence should be addressed. E-mail: olof@chemistry.ucsc.edu. Fax: 831-459-2935. Phone: 831-459-3155.

‡ University of California.

§ University of Illinois.

[1] Abbreviations: *a*, low-spin heme *a*; a^{3+}, oxidized low-spin heme *a*; a^{2+}, reduced low-spin heme *a*; a_3, high-spin heme a_3; a_3^{3+}, oxidized high-spin heme a_3; a_3^{2+}, reduced high-spin heme a_3; Cu_A, the binuclear mixed-valence copper A center; Cu_B, copper B; MVCO, mixed-valence CO-bound oxidase; FRCO, fully reduced CO-bound oxidase; SVD, singular value decomposition; *b*-spectrum, spectral changes associated with a respective first-order process.

10.1021/bi700728g CCC: $37.00
Published on Web 10/12/2007

valence enzyme was biphasic, with the slower phase having somewhat higher amplitude. The apparent acceleration of the true CO binding rate due to the probe beam in single-wavelength experiments and the relationship between the observed and the microscopic rates are discussed.

MATERIALS AND METHODS

Bacterial Growth and Enzyme Purification. The *R. sphaeroides* strain JS 100, containing the histidine-tagged wild-type subunit I gene cloned into an expression vector (*12*), was grown aerobically in Sistrom's media as previously reported (*13*). The cells were harvested and the cytochrome *c* oxidase was purified as previously described (*12*) with the following modifications reported by Hiser et al. (*14*): dodecyl-β-maltopyranoside (DM) was added (final concentration of 3%) to solubilize the purified membranes, and Ni^{2+}-NTA agarose slurry was added to the membrane solution at 1 mL per mg oxidase and the solution was stirred overnight. The enzyme was eluted slowly from the Ni^{2+}-NTA column with 150 mM imidazole in 10 mM Tris-HCl, 40 mM KCl, and 0.1% DM (pH 8.0) (*12*). The imidazole was removed by a buffer exchange with 10 mM KH_2PO_4, 1 mM EDTA, and 0.1% DM (pH 7.6). The enzyme was concentrated, frozen in liquid nitrogen and stored at −80 °C until further use. The total amount of oxidase present in the membranes was estimated from the reduced-minus-oxidized spectrum ($\epsilon_{606-630} = 24$ mM^{-1} cm^{-1}) (*15*). The bovine heart oxidase was isolated according to published procedures (*16*, *17*).

Fully reduced cytochrome *c* oxidase from *R. sphaeroides* or bovine heart was prepared by adding sodium ascorbate (final concentration of 2 mM) and ruthenium hexammine chloride (mediator) (final concentration of 0.25 μM) to a deoxygenated oxidized enzyme solution. Exposure of the resulting solution to CO for ~1 h generated the CO-bound form (FRCO). The final enzyme concentration was 15−20 μM. The mixed-valence CO-bound enzyme (MVCO) was prepared by exposing a deoxygenated enzyme solution to CO for a few hours or overnight. In some cases, ferricyanide was added to reoxidize the fraction of heme *a* that had become reduced upon incubation under CO. The formation of the fully reduced and mixed-valence CO complexes was verified by their Soret and visible spectra (*18*, *19*).

The CO-bound enzyme complexes were photolyzed using the second harmonic (532 nm) pulse from a Q-switched DCR-11 Nd:YAG laser (~7 ns full width at half-maximum). In the single-wavelength detection mode, the transient kinetics in the microsecond-to-second time window were monitored at selected wavelengths using a tungsten lamp as a probe beam and a photomultiplier or photodiode detector (*16*). The signals were recorded by a 500 MHz digital oscilloscope (Le Croy 9350AM). Each kinetic trace was an average of 40 scans. A sum of exponential functions was fitted to the experimental absorbance traces using Matlab (The Mathworks, Inc.) (*16*).

Time-resolved optical absorption difference spectra were recorded in the Soret and visible regions following photolysis of the CO-bound enzyme (*16*, *20*, *21*). The spectrum at each time point was an average of 40 individual spectra, each produced by a single laser pulse. As we have shown recently (*22*), insignificant photoreduction of heme *a* occurs upon single laser pulse photolysis at 532 nm. The data matrix was analyzed by SVD, and the time-dependent **v**-vectors were fitted to a sum of exponential functions, followed by calculation of the wavelength-dependent amplitudes, i.e., the *b*-spectra. The absence of spectral structure in the residuals, the difference between the data and the fit, was used to judge the quality of the fit (*8*, *20*). The sum of the three microsecond *b*-spectra was compared to a model spectrum representing electron back-flow from heme a_3 to heme *a*; the latter was generated from a linear combination of the spectra of the oxidized, reduced, mixed-valence, and fully reduced CO-bound complexes and the Cu_A^{2+} spectrum (*23*). All calculations were carried out using Matlab as previously described (*8*, *10*, *20*, *24*−*26*).

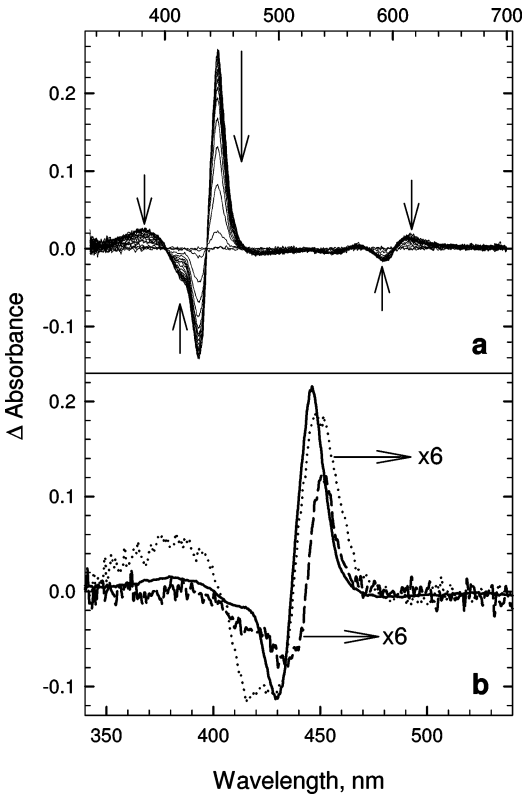

FIGURE 1: (a) Time-resolved optical absorption difference spectra (post- minus prephotolysis) recorded following photodissociation of the fully reduced CO-bound enzyme at room temperature. The data represent both Soret and visible regions, and the arrows indicate progressive time delays. The concentration of the enzyme was 13 μM. The buffer was 50 mM sodium phosphate (pH 7.5). (b) The spectral changes (*b*-spectra) associated with the three-exponential fit to the time-resolved optical data. The apparent lifetimes were 0.9 μs (b_1; dashed), 190 μs (b_2; dotted) and 20 ms (b_3; solid). The b_1 and b_2 spectra have been multiplied by a factor of 6 for an easier comparison with the 20 ms b_3 spectrum.

RESULTS

Fully Reduced CO-Bound (FRCO) R. sphaeroides Cytochrome c Oxidase. In order to study conformational changes accompanying CO release and rebinding in *R. sphaeroides* cytochrome *c* oxidase, we performed flash-photolysis experiments on the FRCO enzyme. Optical absorption changes associated with this reaction were monitored using multi-wavelength detection in the 350−700 nm spectral range. Figure 1a shows time-resolved absorption difference spectra (post- minus prephotolysis) recorded simultaneously in the Soret and visible regions following photolysis of the FRCO

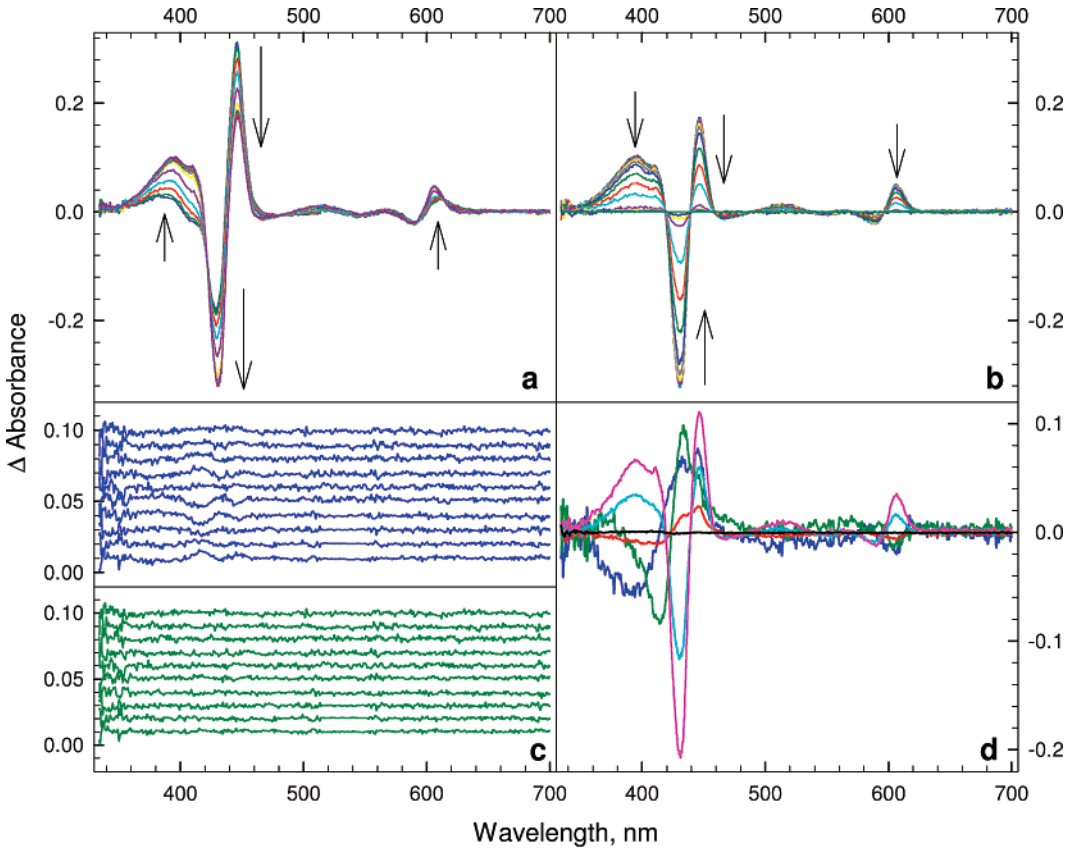

FIGURE 2: (a and b) Time-resolved optical absorption difference spectra (post- minus prephotolysis) recorded at room temperature after photodissociation of the mixed-valence CO-bound enzyme. Panel a represents 13 delay times between 100 ns and 70 μs, and panel b, 16 delay times between 100 μs and 1 s. The arrows indicate progressive time delays. The concentration of the enzyme was 14 μM. The buffer was 50 mM sodium phosphate (pH 7.5). (c) The residuals in the 100 ns to 30 μs time window for the four-exponential fit (blue curves) and five-exponential fit (green curves). (d) The *b*-spectra associated with the apparent lifetimes in the five-exponential fit to the time-resolved data of the fully reduced enzyme: b_1, 1.1 μs (blue); b_2, 2.4 μs (green); b_3, 31 μs (red); b_4, 68 ms (cyan); b_5, 240 ms (magenta).

enzyme. The difference spectra represent 20 delay times, logarithmically spaced between 100 ns and 200 ms. The spectra were analyzed by SVD and global exponential fitting, and three lifetimes, 0.9 μs, 190 μs, and 20 ms, were required to adequately fit the data as judged by the random noise in the residual spectra. The spectral changes (*b*-spectra) associated with the three apparent lifetimes are shown in Figure 1b. The 0.9 and 190 μs *b*-spectra have been multiplied by a factor of 6 for easier comparison with the 20 ms *b*-spectrum. Because of their small amplitude, the *b*-spectra in the visible region are not shown.

The 0.9 μs *b*-spectrum has a minimum at 434 nm, a negative shoulder at ~417 nm, and a well-defined maximum at 450 nm. This process is attributed to a relaxation of the photogenerated heme a_3 based on a similar process (1.5 μs) in the bovine heart enzyme (*8*, *10*). The nature of the conformational change at heme a_3 is unknown, but it occurs on the same time scale as CO dissociation from Cu_B^+ (*8*, *10*, *27*). In cytochrome bo_3 from *Escherichia coli* and in the bovine enzyme, CO ligation changes at Cu_B have been linked to changes in hydrogen bonding to the conserved E286 (*R. sphaeroides* labeling) as shown by FTIR (*28*) and time-resolved FTIR spectroscopy (*29*, *30*), respectively; however, changes in the environment of E286 were not observed upon photolysis of CO from the fully reduced *R. sphaeroides* (*29*, *30*) or *Paracoccus denitrificans* enzyme (*31*). The 190 μs *b*-spectrum displays a rather broad trough with two minima at ~417 and 428 nm and a broad absorbance maximum centered at 448 nm. The common spectral feature at 417 nm in b_1 and b_2 suggests that the 190 μs process may correspond to further relaxation of heme a_3, similar to that suggested for the 200−400 μs process observed in the bovine heart enzyme (*8*, *10*). The *b*-spectrum associated with the 20 ms CO recombination phase has well-defined minimum and maximum at 429 and 446 nm, respectively, and this phase is attributed to the CO recombination to heme a_3. The meaning of the different phases will be addressed in more detail below.

Mixed-Valence CO-Bound (MVCO) R. sphaeroides Cytochrome c Oxidase. Intramolecular electron transfer in *R. sphaeroides* cytochrome oxidase was investigated following flash-photolysis of the MVCO enzyme. In order to obtain spectral information regarding the various intermediates, we monitored the reaction using an intensified diode array. Time-dependent absorption difference spectra (post- minus pre-photolysis) were recorded at 26 delay times ranging from 100 ns to 1 s. For improved accuracy and to monitor possible electron back-flow to Cu_A, the number of time delays was increased from three to six per decade in the 10−100 μs time window. The mixed-valence state of the enzyme was maintained by the addition of ferricyanide. Figure 2 (a and b) shows time-resolved difference spectra between 100 ns and 70 μs and 100 μs and 1 s in the Soret and visible regions, respectively. The arrows indicate the direction of absorbance changes with time. Residuals resulting from a four-exponential fit corresponding to apparent lifetimes of 1.5 μs,

19 μs, 68 ms, and 240 ms showed a deviation from random noise in the early microsecond time window (Figure 2c, top part), which were eliminated when five exponentials, corresponding to apparent lifetimes of 1.1 μs, 2.4 μs, 31 μs, 68 ms, and 240 ms, were used (Figure 2c, bottom part). The associated spectral changes (*b*-spectra) are shown in Figure 2d. In general, two individual sequential processes with 1.1 and 2.4 μs apparent lifetimes are difficult to separate because of closeness in time, and for proper separation, require many more time points than shown in Figure 2. However, even in the case of a few delay times as reported here, improvement in the residuals upon going from a four to a five-exponential fit clearly shows the need for two exponentials on early microsecond time scale (Figure 2c). We believe that the two physical processes responsible for these two exponentials are not sequential but instead occur simultaneously and thus cannot be separated by exponential fitting even if more delay times were recorded in the microsecond time window (see below).

For a sequential scheme, the *b*-spectra represent spectral changes between successive intermediates if the lifetimes are well separated. Under these conditions, positive absorbance bands in a *b*-spectrum represent decaying intermediates, while the negative bands correspond to intermediates being formed. The first three *b*-spectra (blue (b_1), green (b_2), and red (b_3)) associated with the microsecond lifetimes of the five exponential fit (Figure 2d) predominantly reflect absorption changes associated with electron back-flow from heme a_3 to heme *a*; the first two lifetimes, 1.1 and 2.4 μs, most likely contain relaxation or structurally related spectral changes of heme a_3 as well. In the first three *b*-spectra, the large positive lobe around ~430 nm reflects the decay of the oxidized heme *a*, and the large negative absorption below 420 nm is clearly consistent with the formation of oxidized heme a_3. The disappearance of the reduced heme a_3 absorption band at ~445 nm is partially compensated by the appearance of reduced heme *a* because the two hemes have absorption maxima at nearly the same wavelength.

Spectral contribution from the heme a_3 relaxation can be observed when the *b*-spectra associated with the 1.1 μs and 2.4 μs apparent lifetimes are compared (Figure 2d, blue and green spectra, respectively). Although both *b*-spectra show a signature of electron back-flow, they are somewhat different, which suggests that the detailed mechanism of the early microsecond processes may be more complex, involving a simultaneous heme a_3 relaxation and intramolecular electron transfer. Although the two exponentials are real (as indicated by the improvement in the residuals, Figure 2c), the two physical processes cannot be separated in the exponential fitting regardless of the accuracy of the experimental data.

The third *b*-spectrum (31 μs) (Figure 2d, red curve) also indicates electron back-flow but of much smaller amplitude and at a considerably slower rate than the early processes. Whether a fraction of this slower electron back-flow is associated with Cu_A reduction could not be determined based on the spectral change of the hemes alone because of shifts in the heme spectra (see further discussion below). To determine if Cu_A plays a role in the "slow" electron back-flow step, we conducted single-wavelength absorption experiments at 820 nm. We did not detect Cu_A reduction on this time scale in the mixed-valence enzyme, and therefore we conclude that the third *b*-spectrum arises from electron transfer from heme a_3 to heme *a*, perhaps with a more relaxed heme a_3 being involved. The fourth and fifth *b*-spectra (Figure 2d, cyan and magenta curves, respectively), corresponding to the 68 and 240 ms apparent lifetimes, respectively, have practically the same shape, and both reflect a CO rebinding process with relative amplitudes of 0.36 and 0.64, respectively.

We found that only an "over-reduced" sample, i.e., a sample in which a significant amount of heme *a* was reduced, showed the characteristic decrease at 820 nm due to reduction of Cu_A upon intramolecular electron transfer from heme *a* (*4*, *32*). As discussed above, no significant spectral change at 820 nm, beyond that expected due to redox state changes of the hemes (*33*), was observed for the ferricyanide-treated mixed-valence sample (data not shown); the low concentration of ferricyanide (<20 μM) excludes the possibility of a rapid Cu_A reoxidation by ferricyanide. This suggests that electron transfer to Cu_A only takes place if a fraction of heme *a* is reduced in the original sample. This is in agreement with our earlier studies (*32*) and previous studies of Morgan et al. (*4*), who reported no electron transfer from heme *a* to Cu_A in the "pure" mixed-valence enzyme, but only following photolysis of the three-electron-reduced CO-bound enzyme.

DISCUSSION

Spectral Changes of Heme a_3 in the Fully Reduced Enzyme. Are Different CO-Conformers Present? Examination of the first two *b*-spectra resulting from the three-exponential fit of the multichannel data on the fully reduced *R. sphaeroides* enzyme (Figure 1b, dashed (b_1) and dotted (b_2)) reveals a common spectral feature at 420−430 nm in both. Figure 3a shows the first two *b*-spectra, which have been normalized to the absorbance of the negative shoulder at ~420 nm. It appears that the b_1 spectrum (Figure 3a, solid trace) represents a combination of two spectral changes: the first is similar to the b_2 spectrum (Figure 3a, dashed trace), and the second is a result of a blue shift in the absorption spectrum of reduced heme a_3. The presence of a common spectral feature in the first two *b*-spectra indicates that the corresponding process is spread out in time, suggesting that the relaxation process follows a nonexponential or so-called stretched-exponential kinetics. Nonexponential kinetics can be fitted to a sum of exponentials because any monotone function can always be fitted to a sum of exponentials.

We can separate the spectral shift of heme a_3, which dominates the first *b*-spectrum, from the stretched relaxation process (common spectral feature) by taking the difference between b_1 (Figure 3a, solid curve), which includes both processes, and the normalized b_2 (Figure 3a, dashed curve), which contains only the common spectral feature at ~420 nm. Figure 3b shows the difference spectrum, which indeed resembles a blue spectral shift of the reduced heme a_3 absorption band. A blue spectral shift was also observed between intermediates 1 and 2 following photolysis of FRCO bovine heart cytochrome *c* oxidase (*8*).

One interpretation of the above results is that the relaxation of heme a_3 is a nonexponential process for which the early changes are spectrally different from the rest. An alternative explanation would be that the common spectral feature in the first two *b*-spectra arises from one population and the

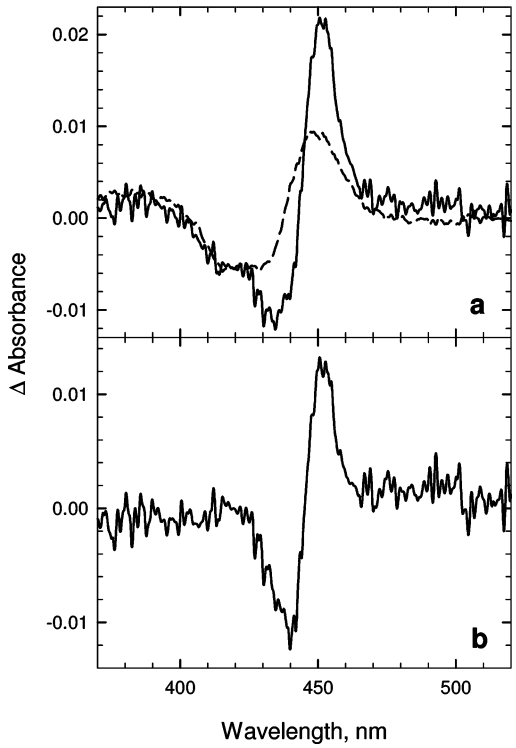

FIGURE 3: (a) The first two *b*-spectra (b_1, 0.9 μs, solid; b_2, 190 μs, dashed) from the three-exponential fit of the time-resolved data of the fully reduced enzyme. The *b*-spectra have been normalized to the absorbance of the negative shoulder at ~420 nm. (b) The difference between the two *b*-spectra (b_1 minus b_2).

pure spectral shift arises from another population of conformationally different molecules. In the latter case, the two different conformers of the reduced CO-bound enzyme must have the same CO recombination kinetics because only one recombination rate (20 ms) is observed. Alternatively, because the spectral changes for both the relaxation and the CO recombination occur in a similar wavelength range, we cannot exclude that the 190 μs *b*-spectrum has contributions from both processes. In this case, the early CO recombination would presumably represent a different CO conformer. The presence of two CO conformers is consistent with previously reported resonance Raman studies (*19*) and FTIR experiments of the conformational substates of FRCO *R. sphaeroides* cytochrome *c* oxidase (*34*).

Comparison of the Postphotolysis Spectra of the Reduced Heme a_3 in the Fully Reduced and the Mixed-Valence Enzyme. Theoretically the first (100 ns) time-resolved difference spectrum (referenced versus the unphotolyzed CO complex) in the CO flash-photolysis experiment of the FRCO enzyme is expected to be the same as the corresponding spectrum of the MVCO enzyme because both represent the heme a_3^{2+}-minus-heme a_3^{2+}-CO difference spectrum. To compare the two experimental spectra accurately, we recorded an additional set of light-induced difference spectra for the FRCO and MVCO enzyme (Figure 4 a−d, green and blue traces, respectively) using a single sample, and thus the same exact enzyme concentration, and the same laser power for the photolysis. A comparison of the two 100 ns difference spectra (Figure 4a and 4b, green and blue traces) with the bench-made reduced-minus-CO difference spectrum (model spectrum) (Figure 4a and 4b, red trace) shows that the 100 ns spectrum of the fully reduced enzyme (green trace) is quite different from the model (red trace), while the mixed-valence 100 ns spectrum (blue trace) is close but not identical to the model spectrum. This indicates that neither 100 ns spectrum corresponds to the fully relaxed state. A comparison of the 100 ns time-resolved difference spectrum of the mixed-valence enzyme (Figure 4c and Figure 4d, blue traces) with the time-resolved difference spectrum of the fully reduced enzyme recorded after relaxation but before CO recombination (2 ms) (green trace) reveals a close resemblance between the two. The similarity between the two suggests that the mixed-valence enzyme either relaxes considerably before 100 ns and thus significantly faster than the reduced enzyme, or it does not have the same unrelaxed form that the fully reduced enzyme has at 100 ns. This may be due to a variety of effects that heme *a* and/or Cu_A can exert on the conformation, ligation state, etc. of the binuclear site (*8*, *35*, *36*).

The difference between the fully reduced and mixed-valence 100 ns time-resolved difference spectra (Figure 4e and Figure 4f, blue traces) does not correspond to the spectral differences expected upon electron transfer from heme a_3 to heme *a* (Figure 4e and Figure 4f, green traces) (*36*, *37*). However, whether the spectral changes represent ultrafast electron transfer between the hemes but are masked by a large spectral contribution arising from the differences in the degree of relaxation between the mixed-valence and fully reduced enzyme on fast time scale, cannot be determined at this point. Ultrafast electron transfer between heme *a* and heme a_3 has been reported for the bovine enzyme with an apparent lifetime of 1.2 ns (*36*, *38*, *39*); a comparison of the picoecond heme a_3-CO photodissociation spectra for the mixed-valence and fully reduced enzyme indicated significant spectral interactions between the hemes under different redox states of heme *a* (*36*).

As mentioned above, the 1.1 and 2.4 μs processes for the MVCO enzyme are difficult to resolve and both contain spectral changes due to heme a_3 relaxation and electron backflow. The 1.1 μs process in the mixed-valence enzyme, as in the fully reduced enzyme, occurs on the same time scale as the CO dissociation from Cu_B in the bovine enzyme (*27*, *40*). Changes in the FTIR redox difference spectra of the *R. sphaeroides* and *P. denitrificans* aa_3 (*30*, *41*) and cytochrome bo_3 (*42*) and in the FTIR or time-resolved FTIR photolysis spectra of the MVCO bovine oxidase (*43*, *44*) and the *Paracoccus* enzyme (*31*) have been associated with conformational/protonation state changes at E286. Thus the intramolecular electron transfer may be induced by the relaxation in the vicinity of heme a_3, perhaps by changes in the environment of E286 triggered by the dissociation of CO from Cu_B (*36*, *38*). This supports the observation that the first two microsecond processes involving both heme a_3 relaxation and the intramolecular heme−heme electron transfer are intricately linked and perhaps occur simultaneously and not sequentially.

The first two microsecond *b*-spectra reported here for the photolysis of the mixed-valence *R. sphaeroides* enzyme are not identical to those previously reported for the bovine heart enzyme (*8*, *10*). We do not expect the corresponding *b*-spectra between the mammalian and bacterial enzymes to be identical because the back-flow is much larger in the latter and the contributions from relaxations are also different. Moreover, in both enzymes, the apparent lifetimes of the

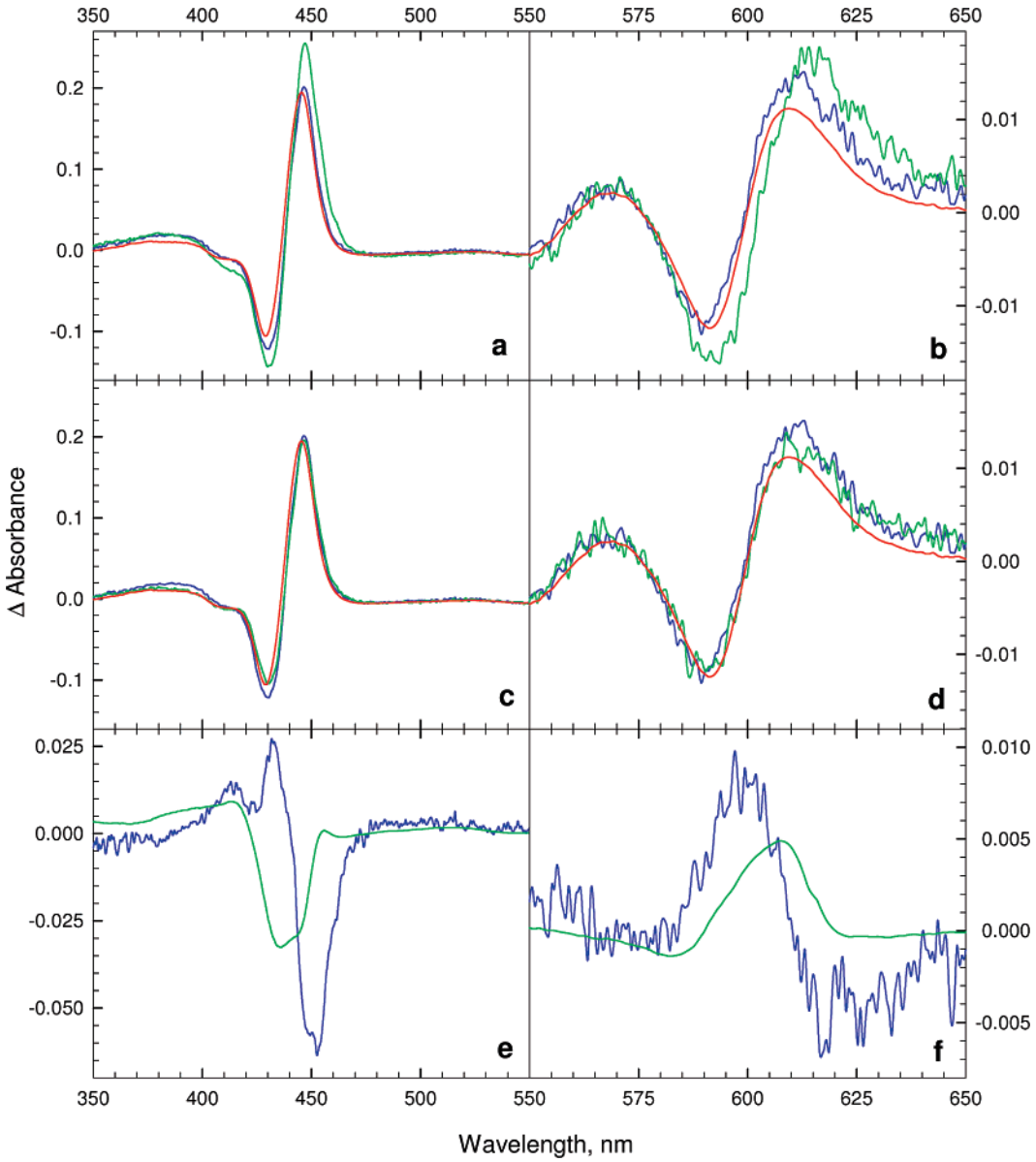

FIGURE 4: (a and b) A comparison of the 100 ns time-resolved difference spectra recorded following photolysis of CO from heme a_3 of the fully reduced enzyme (green traces) and mixed-valence enzyme (blue traces) in the Soret (a) and visible (b) regions. The red traces represent the model bench-made reduced-minus-CO difference spectrum. (c and d) The time-resolved difference spectra of the mixed-valence (blue traces) and fully reduced enzyme (green traces) recorded 100 ns and 2 ms after CO photolysis, respectively. The red traces represent the model bench-made reduced-minus-CO difference spectrum. (e and f) A comparison of the difference between the fully reduced and mixed-valence 100 ns time-resolved difference spectra (blue curves) displayed in panels a and b with the spectral changes expected upon electron transfer from heme a_3 to heme *a* (green curves) (see text for details).

first two microsecond processes are so close to each other that the *b*-spectra associated with these lifetimes cannot be interpreted as pure transitions (differences between intermediate spectra). In the case of close lifetimes, all intermediates in that time window contribute significantly to the *b*-spectra and the extent of each intermediate contribution depends on the details of the kinetic scheme (*26*).

The Extent of Electron Back-Flow. Because the three microsecond *b*-spectra of the mixed-valence enzyme are associated with electron back-flow, the total back-flow can be best determined based on the sum of the first three *b*-spectra, hereafter referred to as the b_{123}-spectrum. A detailed mathematical treatment of evaluation of the electron back-flow and the associated spectral changes is given in Appendix 1 (Supporting Information). As mentioned above, the combined *b*-spectrum also contains spectral changes due to heme a_3 relaxation, which cannot be separated from the electron back-flow in the absence of a detailed kinetic scheme, but can be accounted for or largely eliminated as described below. The b_{123}-spectrum can be compared with a model spectrum representing the electron back-flow, which is generated by the sum of the oxidized-minus-reduced heme *a* and reduced-minus-oxidized heme a_3 difference spectra. The former was generated by subtracting the FRCO spectrum from that of the MVCO spectrum. To ensure that 100% of the MVCO state was indeed formed, a sample in which all the heme a_3 had CO bound was generated and subsequently the amount of heme *a* that had become reduced was reoxidized with ferricyanide. The difference spectrum for heme a_3 was constructed by subtracting the bench-made oxidized-minus-CO heme a_3 spectrum (oxidized spectrum minus the mixed-valence CO spectrum) from the reduced-

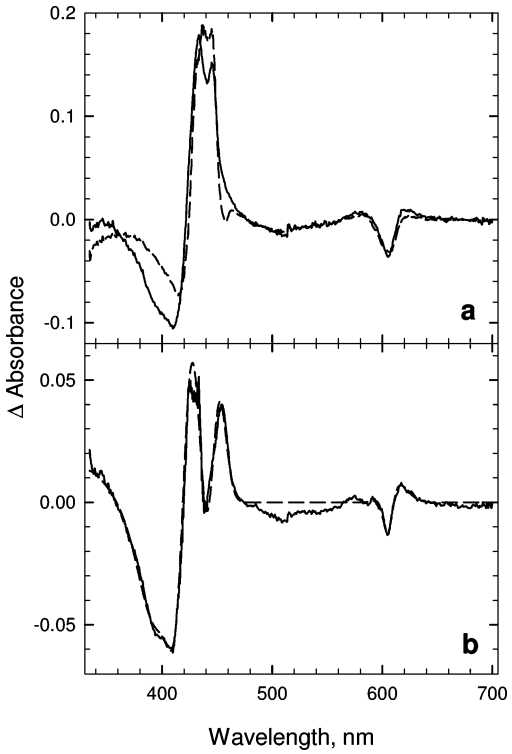

FIGURE 5: (a) A comparison between the b_{123}-spectrum (the sum of the microsecond mixed-valence *b*-spectra; solid trace) and the model spectrum (assuming 100% back-flow; dashed traces). (b) (Solid curve) The double difference spectrum of the back-electron transfer: the b_{123}-spectrum minus the 75% back-flow bench-made model spectrum. The model spectrum was generated by the sum: $(a_3^{2+} - a_3^{3+}) + (a^{3+} - a^{2+})$ assuming 75% back-electron transfer from heme a_3^{2+} to heme a^{3+}. (Dashed curve) A simulation of the double difference spectrum obtained by shifting a pair of composite Gaussian spectra (see text for details).

minus-reduced CO-bound heme a_3 spectrum obtained in our mixed-valance photolysis experiment, i.e., the first (100 ns) intermediate spectrum. By using the experimental, unrelaxed heme a_3 spectrum instead of the bench-made reduced-minus-CO-bound heme a_3 model spectrum, the spectral contribution due to relaxation of heme a_3 present in the b_{123}-spectrum is included in the model spectrum.

The comparison between the b_{123}-spectrum and the model spectrum (assuming 100% back-flow) is shown in Figure 5a (solid and dashed curves, respectively). It is clear that the experimental and model spectra have different shapes, specifically in the 400 nm range where the oxidized heme a_3 absorbs. We cannot accurately determine the extent of the electron back-flow because of the spectral dissimilarities, but we can obtain a reasonable estimate from the 440−450 nm region which is the farthest removed from the altered oxidized heme a_3 absorption band. Figure 5a clearly illustrates the necessity of the multiwavelength approach in kinetic studies. Because of the spectral shift, single-wavelength measurements in the Soret region would give very different estimates of electron back-flow depending on the wavelength of detection. For example, an estimate based on monitoring at 400 nm using previously published extinction coefficients would suggest 200% back-flow. Only in the narrow spectral region around 440 nm would we find consistent and meaningful values for the extent of back-flow, which coincidentally is the wavelength at which previous electron transfer has been monitored (*11*). We estimate the total electron back-flow to be 75%, with 65% taking place on 1−3 μs time scale and 10% on ∼30 μs time scale. This is roughly three times higher than the value determined for the bovine heart cytochrome *c* oxidase (*8*), in agreement with previous observations on the *R. sphaeroides* enzyme, which were based on absorbance changes measured at 444 nm (*11*).

Shifts in Spectra of Oxidized Heme a_3 and Reduced Heme a. In order to investigate the deviations between the heme spectra and the model spectra, we first subtracted 75% of the electron back-flow model spectrum (Figure 5a, dashed line) from the b_{123}-spectrum (Figure 5a, solid line). This approach eliminates 75% of possible relaxation processes occurring concurrently with the intramolecular electron transfer, leaving only 25% or less of the total relaxation contributions unaccounted for (see Appendix 1). This is acceptable because the relaxation is not the major component of the spectral change on microsecond time scale. The shape of the resulting double difference spectrum (Figure 5b, solid curve) in the Soret region is consistent with two difference spectra originating from spectral shifts and superimposed on each other, one centered around 410−420 nm and another centered around 440−450 nm. We assign the first one to oxidized heme a_3 and the latter to reduced heme *a* based on the location of their absorption bands (*45*) and the fact that these are the two heme redox states generated upon electron back-flow.

Our strategy for determining the altered oxidized-minus-reduced heme a_3 and heme *a* difference spectra is based on the assumption that the deviation between the b_{123}-spectrum and the model spectrum representing the electron back-flow between the two hemes is due to spectral shifts. We have simulated the experimental double difference spectrum based on the absorbance maxima and the bandwidth of the absolute spectra of oxidized heme a_3 and reduced heme *a* reported by Vanneste (*45*). According to Vanneste, the oxidized heme a_3 absorption band is relatively broad and has a peak at 414 nm. We modeled the shift in the oxidized heme a_3 spectrum using the sum of two Gaussian curves, which were shifted from 413 and 422 nm to 410 and 418 nm, respectively. The reduced heme *a* spectral shift was modeled by a single Gaussian band shifted from 448 to 445 nm. The difference in the visible region appears to be much smaller, and less accurate to be treated reliably. The experimental double difference spectrum in Figure 5b (solid line) was thus reproduced by combining the difference spectra resulting from the shifted Gaussian bands (Figure 5b, dashed line). The widths and amplitudes of the Gaussian spectra were also slightly adjusted to obtain a good fit.

The difference spectra of the shifted Gaussians for the oxidized heme a_3 and reduced heme *a* were combined with the bench-made model spectra of oxidized-minus-reduced heme a_3 and reduced-minus-oxidized heme *a*, respectively, to produce the shifted difference spectra for the two hemes. The mathematical description of this analysis is detailed in Appendix 1. Figure 6 (solid and dash−dot−dot) shows the shifted difference spectra for the reduced-minus-oxidized heme *a* and oxidized-minus-reduced heme a_3, respectively, compared with the corresponding original (nonshifted) bench-made difference spectra of heme *a* (Figure 6d, dotted curve) and heme a_3 (Figure 6, dashed curve). Although the blue shift in the absolute spectra of both oxidized heme a_3 and reduced heme *a* is similar, ∼3−4 nm, it has a significantly

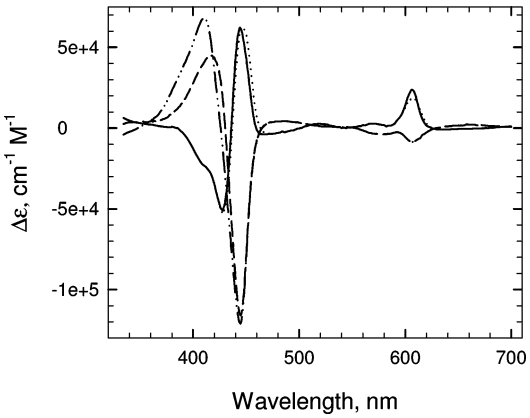

FIGURE 6: A comparison between the shifted and original (nonshifted) bench-made reduced-minus-oxidized heme *a* and oxidized-minus-reduced heme a_3 difference spectra. The solid and dotted curves represent the shifted and nonshifted reduced-minus-oxidized heme *a* difference spectra and the dash−dot−dot and dashed curves represent the shifted and nonshifted oxidized-minus-reduced heme a_3 difference spectra, respectively.

larger effect on the heme a_3 oxidized-minus-reduced difference spectrum than on the heme *a* reduced-minus-oxidized difference spectrum. This is because the shift in the oxidized heme a_3 spectrum decreases the overlap between the reduced and oxidized spectra of heme a_3, whereas the shift in the spectrum of reduced heme *a* increases the overlap between the reduced and oxidized spectra of heme *a*. Note that although the reduced heme *a* spectrum had to be shifted during the simulation, the 440−450 nm spectral range still appears to have been a fairly good choice for making a reasonable estimate of the extent of electron back-flow. The uncertainty in determining the extent of electron back-flow has practically no effect on the extent of the blue shift. We tested 70 and 80% back-flow and found the same shifts; only the amplitudes of the shifted spectra changed slightly.

The simplest explanation for the shift in the absorption spectrum of one heme would be the charge of the other heme, i.e., the electrostatic influence of one heme on the spectrum of the other. However, this is unlikely because the charge on heme *a* decreases by one while the charge on heme a_3 increases by one upon electron back-flow, and yet the spectra of both hemes are blue-shifted by roughly the same amount (3−4 nm). A more plausible explanation is that the transfer of the electron, and perhaps its compensating charge, induces or is accompanied by a certain structural change located somewhere between the hemes, perhaps at E286 (*30*, *41*). Such structural change would influence the spectra of the two hemes equally. Other factors than the oxidation state of the hemes may also have a significant effect on the enzyme properties. For example, the resting and pulsed forms of the oxidized enzyme are both spectrally and kinetically different, possibly due to conformational differences. Early studies based on ligand inhibition (CN^-, NO, and formate) of heme a_3 and Cu_B have indicated metal−metal interactions, which affected the reduced-minus-oxidized spectrum of heme *a* (*35*).

The Effect of Probe Light Intensity on the Apparent Rate of CO Recombination. Ädelroth and co-workers reported a CO recombination rate of 15 s^{-1} (67 ms) for the mixed-valence *R. sphaeroides* oxidase using single wavelength detection (*11*). However, they noted that a smaller, slower second component might also be present. In contrast, the 68 and 240 ms *b*-spectra (Figure 2d, cyan and magenta, respectively) in the mixed-valence flash-photolysis experiment, which are both due to CO recombination, show that the slower process has a larger amplitude (almost twice) than the faster one. The simplest and most plausible explanation for the discrepancies between our multiwavelength and the published single-wavelength results (*11*) is that the continuous probe light exposure in the single-wavelength experiments generates a steady state in which a fraction of the sample is already photolyzed before the laser initiates the reaction. The recovery time and the amplitude of the signal for a steady-state system are dependent on the fraction photolyzed by the probe beam. How the measured apparent rates and amplitudes differ from the true values depends on the details of the kinetic scheme involved. There is no universal way of predicting the probe beam artifact quantitatively, and each case should be analyzed individually based on the underlying kinetic scheme. The validity of the analysis can be tested by comparing the predictions of the analysis with experimental results obtained at different probe light intensity. Note that our normal probe beam is photoactive only in the case of CO recombination in the MVCO enzyme but does not induce any artifact in other types of experiments, e.g., FRCO recombination, because in the latter, the CO recombination rate is "too fast" (∼20 ms compared to 68 and 240 ms in the MVCO photolysis experiment).

In order to test our explanation for the discrepancies between the published recovery rates and amplitudes and our multiwavelength results, we carried out a detailed analysis of the probe beam artifact. First, we conducted single-wavelength experiments with variable light (probe beam) intensities to demonstrate the effects of the probe beam. Figure 7 (solid traces) shows experimental transient kinetic traces at 592 nm on millisecond time scale recorded following photolysis of the MVCO enzyme using our normal probe beam (referred to as ''higher'' probe intensity; panel a) and in the presence of an additional OD 1 neutral density filter (lower probe intensity; panel b). The data are presented on a logarithmic time scale. The smooth lines on top of the experimental traces represent a two-exponential fit; the residuals are shown at the top of the panels. The dash−dot−dash and dashed curves represent the individual exponential components, fast and slow, respectively, at the higher (panel a) and lower (panel b) probe light intensities. It is clear from Figure 7 that the slow component is affected much more in both amplitude and rate by the light intensity than the faster one. The rates for the slow component increased from 208 to 133 ms and the amplitude decreased by 40% with increasing light intensity, whereas for the faster component, the rate increased from 68 ms to 58 ms and the amplitude decreased by 20%. Note that even with the lower light intensity, the slower rate at 592 nm (208 ms) is not as slow as the one observed using the multiwavelength detection (240 ms). This indicates that even with the OD 1 filter, our single-wavelength measuring beam is probably not optimal.

As a second step, we analyzed quantitatively the apparent increase in the observed CO rebinding rate with increased probe beam intensity by using a simplified chemical scheme (Scheme 1), which is based on 75% electron back-flow. In Scheme 1, electron back-flow from heme a_3 to heme *a* is represented by a single reversible reaction, and the photolysis

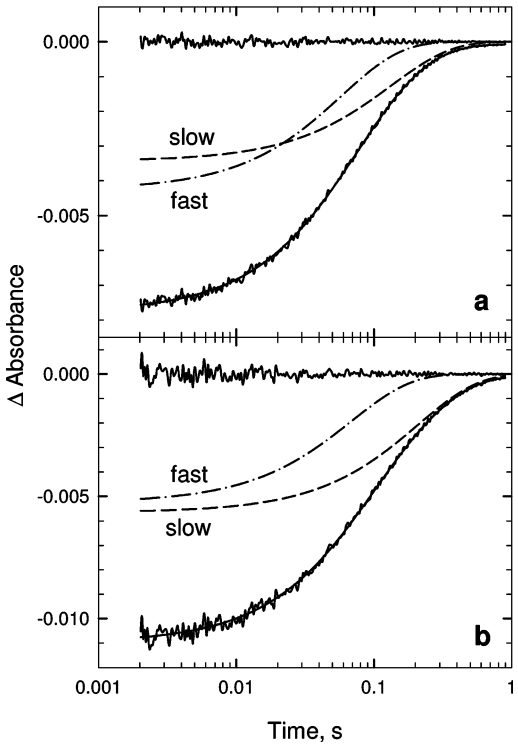

FIGURE 7: Transient kinetic absorption traces at 592 nm recorded during the mixed-valence CO-recombination process (millisecond time scale). (a) Data recorded without a neutral density filter (higher probe light intensity). (b) Data recorded with an OD 1 neutral density filter (lower probe light intensity). The smooth lines on top of the experimental traces represent two-exponential fit to the data corresponding to apparent lifetimes of 68 and 240 ms (panel a) and 133 and 58 ms (panel b). The residuals, the difference between the data and the fit, are shown at the top of the panels. The dash−dot and dashed curves represent the individual exponential components, fast and slow, respectively, at the higher (a) and lower (b) probe light intensities.

Scheme 1: Proposed Scheme for the Light-Dependent CO Recombination in the Mixed-Valence *R. sphaeroides* aa_3 Oxidase[a]

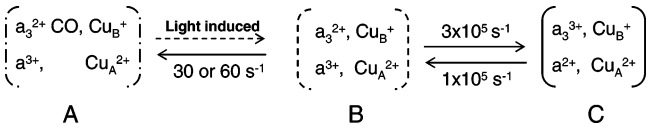

[a] The broken arrow indicates the light-induced process.

and CO recombination together make up the second reversible step. The microscopic rates in Scheme 1 reflect a 3:1 ratio (75%) of the reduced heme *a* (oxidized heme a_3) to oxidized heme *a* (reduced heme a_3), and the sum of the forward and backward rates in the back-flow step corresponds to 2.5 μs. It is assumed that the two experimental CO recombination rates belong to two enzyme populations, and we apply the scheme to each one. The microscopic rate of CO rebinding for the fast component is 60 s^{-1}, which is very close to the one observed for the fully reduced enzyme (50 s^{-1}).

We calculated the relative concentrations of the different intermediates as a function of time for the lower probe beam intensity (OD 1 filter) and for the higher probe beam intensity (no filter). Figure 8 shows the progression during one CO recombination cycle following the laser pulse, and it demonstrates the effect of probe light intensity on the amplitude of the single-wavelength signals (relative concentrations of the intermediates in Scheme 1) and the apparent recovery rates. The slow and fast recovery components are treated separately here as mentioned above. In each case we assumed 50% photolysis of the sample by the laser pulse. Panels a and b in Figure 8 refer to the lower intensity probe beam (Scheme 1, light-induced rate = 0) for the slow and fast components, respectively. Panels c and d represent the slow and fast components for the higher probe beam intensity

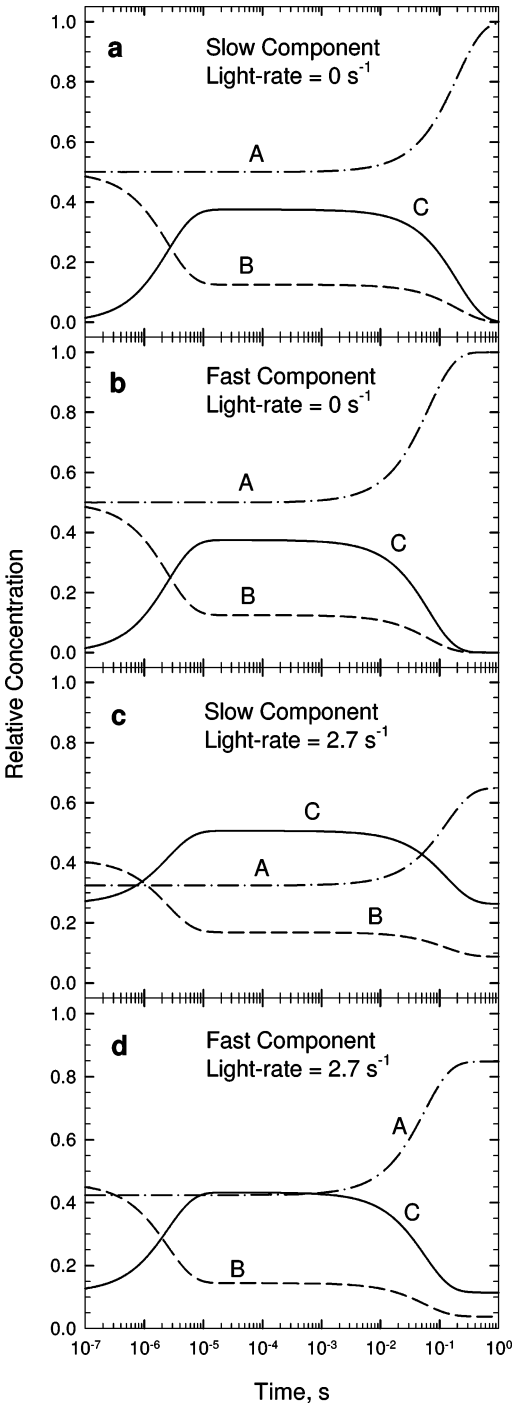

FIGURE 8: Concentration profiles of different intermediates in Scheme 1 upon CO flash-photolysis of the mixed-valence *R. sphaeroides* aa_3 oxidase. The dash−dot, dashed, and solid lines in the concentration profiles represent the first (A), second (B), and the third (C) intermediates in Scheme 1, respectively. Panels a (slow component) and b (fast component) show the relative concentrations of the intermediates using the OD 1 filter, whereas panels c (slow component) and d (fast component) show the relative concentrations of the intermediates in the absence of the neutral density filter.

(light-induced rate = 2.7 s^{-1}), respectively. It is clear that the probe light produces steady-state photolysis. A comparison of panels a and b with c and d shows that the more the probe light depletes the sample, the less CO-bound enzyme is available to be photolyzed by the laser, and the more the recovery appears to speed up. The initial amplitude (Figure 8, curve A) drops by 16% and 36% for the fast and slow components, respectively, for the higher probe beam intensity. The slow CO recombination rate becomes 133 ms (Figure 8c) compared to 208 ms (Figure 8a), and the fast rate changes from 68 ms (Figure 8b) to 58 ms (Figure 8d) when the higher probe beam intensity is used. The scheme used here adequately describes the decrease of the apparent lifetimes (rates) and the change in amplitudes of the intermediates caused by a photoactive probe beam in our single-wavelength experiments. Our analysis predicts that the probe beam reduces the contribution of the slow recovery process relative to the faster one, which at certain wavelengths can reach such a level that the recovery step could reasonably be fitted to a single exponential. The risk in eliminating the slower step is greatest in the Soret region where the absorbance is very high, and even reasonably low intensity probe beam would be able to photolyze the sample at a rate comparable to the very slow sample recovery. This problem is practically absent in a multiwavelength detection experiment, which utilizes microsecond probe light pulses.

CONCLUSIONS

We conclude that heme a_3 in the mixed-valence *R. sphaeroides* cytochrome *c* oxidase is more relaxed or relaxes considerably faster following CO photolysis than the fully reduced enzyme. The difference is most likely related to the effect of the oxidation states of heme *a* and/or Cu_A on the conformation of the binuclear center or their influence on the rate of the conformational change (*8*). The electron back-flow from heme a_3 to heme *a* in the mixed-valence enzyme occurs during three processes on a microsecond time scale, and in agreement with previous studies (*11*), the electron back-flow is ~75%, significantly larger than in the bovine heart enzyme. A comparison of the spectral changes associated with the three microsecond processes and the expected spectral changes associated with the electron back-flow from heme a_3 to heme *a* revealed significant shifts in the absolute spectra of the oxidized heme a_3 and reduced heme *a*, which were determined by simulation using Gaussian curves. To our knowledge, our study is the first to address the issue of spectral shifts of the individual hemes in *R. sphaeroides* and the consequences on the interpretation of the absorbance changes as a measure of back-flow. Because of the shifts in the spectra of the hemes, detection of the electron back-flow in single-wavelength experiments becomes highly unreliable at many of the wavelengths. The spectral shifts may arise from the direct effects of the redox state of one heme on the spectrum of the other, or what is more likely, indirectly via structural control, perhaps through changes in the environment of E286. The observed spectral shifts may reflect structural change that is integral to electron transfer and hence enzyme function. We also found that the CO recombination in the mixed-valence enzyme is biphasic, indicating the presence of two conformers. The absence of the slower recovery component in previous single-wavelength experiments (*11*) can be quantitatively explained by a mechanism based on the establishment of a photoinduced steady state, leading to faster recovery.

SUPPORTING INFORMATION AVAILABLE

Appendix 1 presenting calculation of the shifted heme spectra. This material is available free of charge via the Internet at http://pubs.acs.org.

REFERENCES

1. Boelens, R., and Wever, R. (1979) Electron-transfer processes in carboxy-cytochrome *c* oxidase after photodissociation of cytochrome a_3^{2+}-CO, *Biochim. Biophys. Acta 547*, 296−310.
2. Boelens, R., Wever, R., and Van Gelder, B. F. (1982) Electron transfer after flash photolysis of mixed-valence carboxy cytochrome *c* oxidase, *Biochim. Biophys. Acta 682*, 264−272.
3. Brzezinski, P., and Malmström, B. G. (1987) The mechanism of electron gating in proton pumping cytochrome *c* oxidase: the effect of pH and temperature on internal electron transfer, *Biochim. Biophys. Acta 894*, 29−38.
4. Morgan, J. E., Li, P. M., Jang, D.-J., El-Sayed, M. A., and Chan, S. I. (1989) Electron transfer between cytochrome *a* and copper A in cytochrome *c* oxidase: A perturbed equilibrium study, *Biochemistry 28*, 6975−6983.
5. Oliveberg, M., and Malmström, B. G. (1991) Internal electron transfer in cytochrome *c* oxidase: Evidence for a rapid equilibrium between cytochrome *a* and the bimetallic site, *Biochemistry 30*, 7053−7057.
6. Einarsdóttir, Ó., Dawes, T. D., and Georgiadis, K. E. (1992) New transients in the electron-transfer dynamics of photolyzed mixed-valence CO-cytochrome *c* oxidase, *Proc. Natl. Acad. Sci. U.S.A. 89*, 6934−6937.
7. Verkhovsky, M. I., Morgan, J. E., and Wikström, M. (1992) Intramolecular electron transfer in cytochrome *c* oxidase: A cascade of equilibria, *Biochemistry 31*, 11860−11863.
8. Georgiadis, K. E., Jhon, N.-I., and Einarsdóttir, Ó. (1994) Time-resolved optical absorption studies of intramolecular electron transfer in cytochrome *c* oxidase, *Biochemistry 33*, 9245−9256.
9. Hallén, S., Brzezinski, P., and Malmström, B. G. (1994) Internal electron transfer in cytochrome *c* oxidase is coupled to protonation of a group close to the bimetallic site, *Biochemistry 33*, 1467−1472.
10. Einarsdóttir, Ó., Georgiadis, K. E., and Sucheta, A. (1995) Intramolecular electron transfer and conformational changes in cytochrome *c* oxidase, *Biochemistry 34*, 496−508.
11. Ädelroth, P., Brzezinski, P., and Malmström, B. G. (1995) Internal electron transfer in cytochrome *c* oxidase from *Rhodobacter sphaeroides*, *Biochemistry 34*, 2844−2849.
12. Mitchell, D. M., and Gennis, R. B. (1995) Rapid purification of wildtype and mutant cytochrome *c* oxidase from *Rhodobacter sphaeroides* by Ni^{2+}-NTA affinity chromatography, *FEBS Lett. 368*, 148−150.
13. Zhen, Y., Qian, J., Follmann, K., Hayward, T., Nilsson, T., Dahn, M., Hilmi, Y., Hamer, A. G., Hosler, J. P., and Ferguson-Miller, S. (1998) Overexpression and purification of cytochrome *c* oxidase from *Rhodobacter sphaeroides*, *Protein Expression Purif. 13*, 326−336.
14. Hiser, L., Di Valentin, M., Hamer, A. G., and Hosler, J. P. (2000) Cox11p is required for stable formation of the Cu(B) and magnesium centers of cytochrome *c* oxidase, *J. Biol. Chem. 275*, 619−23.
15. Hosler, J. P., Fetter, J., Tecklenburg, M. M. J., Espe, M., Lerma, C., and Ferguson-Miller, S. (1992) Cytochrome aa_3 of *Rhodobacter sphaeroides* as a model for mitochondrial cytochrome *c* oxidase—purification, kinetics, proton pumping, and spectral analysis, *J. Biol. Chem. 267*, 24264−24272.
16. Szundi, I., Cappuccio, J., and Einarsdóttir, Ó. (2004) Amplitude analysis of single-wavelength time-dependent absorption data does not support the conventional sequential mechanism for the reduction of dioxygen to water catalyzed by bovine heart cytochrome *c* oxidase, *Biochemistry 43*, 15746−15758.
17. Yoshikawa, S., Choc, M. G., O'Toole, M. C., and Caughey, W. S. (1977) An infrared study of CO binding to heart cytochrome *c* oxidase and hemoglobin A, *J. Biol. Chem. 252*, 5498−5508.

18. Brzezinski, P., and Malmström, B. G. (1985) The reduction of cytochrome *c* oxidase by carbon monoxide, *FEBS Lett. 187*, 111−114.
19. Wang, J., Takahashi, S., Hosler, J. P., Mitchell, D. M., Ferguson-Miller, S., Gennis, R. B., and Rousseau, D. L. (1995) Two conformations of the catalytic site in the aa_3-type cytochrome *c* oxidase from *Rhodobacter sphaeroides*, *Biochemistry 34*, 9819−9825.
20. Sucheta, A., Szundi, I., and Einarsdóttir, Ó. (1998) Intermediates in the reaction of fully reduced cytochrome *c* oxidase with dioxygen, *Biochemistry 37*, 17905−17914.
21. Paula, S., Sucheta, A., Szundi, I., and Einarsdóttir, Ó. (1999) Proton and electron transfer during the reduction of molecular oxygen by fully reduced cytochrome *c* oxidase: A flow-flash investigation using optical multichannel detection, *Biochemistry 38*, 3025−3033.
22. Winterle, J. S., and Einarsdóttir, Ó. (2006) Photoreactions of cytochrome *c* oxidase, *Photochem. Photobiol. 82*, 711−719.
23. Slutter, C. E., Sanders, D., Wittung, P., Malmström, B. G., Aasa, R., Richards, J. H., Gray, H. B., and Fee, J. A. (1996) Water-soluble recombinant Cu_A-domain of the cytochrome ba_3 from subunit II from *Thermus thermophilus*, *Biochemistry 35*, 3387−3395.
24. Sucheta, A., Georgiadis, K. E., and Einarsdóttir, Ó. (1997) Mechanism of cytochrome *c* oxidase-catalyzed reduction of dioxygen to water. Evidence for peroxy and ferryl intermediates at room temperature, *Biochemistry 36*, 554−565.
25. Van Eps, N., Szundi, I., and Einarsdóttir, Ó. (2003) pH dependence of the reduction of dioxygen to water by cytochrome *c* oxidase. 1. The P_R state is a pH-dependent mixture of three intermediates, A, P, and F, *Biochemistry 42*, 5065−5073.
26. Szundi, I., Van Eps, N., and Einarsdóttir, Ó. (2003) pH dependence of the reduction of dioxygen to water by cytochrome *c* oxidase. 2. Branched electron transfer pathways linked by proton transfer, *Biochemistry 42*, 5074−5090.
27. Einarsdóttir, Ó., Dyer, R. B., Lemon, D. D., Killough, P. M., Hubig, S. M., Atherton, S. J., López-Garriga, J. J., Palmer, G., and Woodruff, W. H. (1993) Photodissociation and recombination of carbonmonoxy cytochrome oxidase: Dynamics from picoseconds to kiloseconds, *Biochemistry 32*, 12013−12024.
28. Puustinen, A., Bailey, J. A., Dyer, R. B., Mecklenburg, S. L., Wikström, M., and Woodruff, W. H. (1997) Fourier transform infrared evidence for connectivity between Cu_B and glutamic acid 286 in cytochrome bo_3 from *Escherichia coli*, *Biochemistry 36*, 13195−200.
29. Gennis, R. B. (2003) Some recent contributions of FTIR difference spectroscopy to the study of cytochrome oxidase, *FEBS Lett. 555*, 2−7.
30. Heitbrink, D., Sigurdson, H., Bolwien, C., Brzezinski, P., and Heberle, J. (2002) Transient binding of CO to Cu_B in cytochrome *c* oxidase is dynamically linked to structural changes around a carboxyl group: A time-resolved step-scan Fourier transform infrared investigation, *Biophys. J. 82*, 1−10.
31. Rost, B., Behr, J., Hellwig, P., Richter, O. M., Ludwig, B., Michel, H., and Mäntele, W. (1999) Time-resolved FT-IR studies on the CO adduct of *Paracoccus denitrificans* cytochrome *c* oxidase: comparison of the fully reduced and the mixed valence form, *Biochemistry 38*, 7565−7571.
32. Einarsdóttir, Ó., Georgiadis, K. E., and Dawes, T. D. (1992) Evidence for a band III analogue in the near-infrared absorption spectra of cytochrome *c* oxidase, *Biochem. Biophys. Res. Commun. 184*, 1035−1041.
33. Szundi, I., Liao, G.-L., and Einarsdóttir, Ó. (2001) Near-infrared time-resolved optical absorption studies of the reaction of fully reduced cytochrome *c* oxidase with dioxygen, *Biochemistry 40*, 2332−2339.
34. Mitchell, D. M., Müller, J. D., Gennis, R. B., and Nienhaus, G. U. (1996) FTIR study of conformational substates in the CO adduct of cytochrome *c* oxidase from *Rhodobacter sphaeroides*, *Biochemistry 35*, 16782−16788.
35. Blair, D. F., Bocian, D. F., Babcock, G. T., and Chan, S. I. (1982) Evidence for modulation of the heme absorptions of cytochrome *c* oxidase by metal-metal interactions, *Biochemistry 21*, 6928−6935.
36. Pilet, E., Jasaitis, A., Liebl, U., and Vos, M. H. (2004) Electron transfer between hemes in mammalian cytochrome *c* oxidase, *Proc. Natl. Acad. Sci. U.S.A. 101*, 16198−16203.
37. Namslauer, A., Branden, M., and Brzezinski, P. (2002) The rate of internal heme-heme electron transfer in cytochrome *c* oxidase, *Biochemistry 41*, 10369−10374.
38. Jasaitis, A., Rappaport, F., Pilet, E., Liebl, U., and Vos, M. H. (2005) Activationless electron transfer through the hydrophobic core of cytochrome *c* oxidase, *Proc. Natl. Acad. Sci. U.S.A. 102*, 10882−10886.
39. Verkhovsky, M. I., Jasaitis, A., and Wikström, M. (2001) Ultrafast haem-haem electron transfer in cytochrome *c* oxidase, *Biochim. Biophys. Acta 1506*, 143−146.
40. Dyer, R. B., Einarsdóttir, Ó., Killough, P. M., López-Garriga, J. J., and Woodruff, W. H. (1989) Transient binding of photodissociated CO to Cu_B^+ of eukaryotic cytochrome oxidase at ambient temperature. Direct evidence from time-resolved infrared spectroscopy, *J. Am. Chem. Soc. 111*, 7657−7659.
41. Hellwig, P., Rost, B., and Mäntele, W. (2001) Redox dependent conformational changes in the mixed valence form of the cytochrome *c* oxidase from *P. denitrificans*, *Spectrochim. Acta Part A 57*, 1123−1131.
42. Lübben, M., Prutsch, A., Mamat, B., and Gerwert, K. (1999) Electron transfer induces side-chain conformational changes of glutamate-286 from cytochrome bo_3, *Biochemistry 38*, 2048−2056.
43. McMahon, B. H., Fabian, M., Tomson, F., Causgrove, T. P., Bailey, J. A., Rein, F. N., Dyer, R. B., Palmer, G. P., Gennis, R. B., and Woodruff, W. H. (2004) FTIR studies of internal proton transfer reactions linked to inter-heme electron transfer in bovine cytochrome *c* oxidase, *Biochim. Biophys. Acta 1655*, 321−331.
44. Okuno, D., Iwase, T., Shinzawa-Itoh, K., Yoshikawa, S., and Kitagawa, T. (2003) FTIR detection of protonation/deprotonation of the key carboxyl side chains caused by redox change of the Cu_A-heme *a* moiety and ligand dissociation from the heme a_3-Cu_B center of bovine heart cytochrome *c* oxidase, *J. Am. Chem. Soc. 125*, 7209−7218.
45. Vanneste, W. H. (1966) The stoichiometry and absorption spectra of components *a* and a_3 in cytochrome *c* oxidase, *Biochemistry 5*, 838−848.

BI700728G